BIOCHEMISTRY

 Volume 45, Number 36 September 12, 2006

Articles

Solution NMR and Computer Simulation Studies of Active Site Loop Motion in Triosephosphate Isomerase†

Francesca Massi, Chunyu Wang,‡ and Arthur G. Palmer, III*

Department of Biochemistry and Molecular Biophysics, Columbia University, 630 West 168th Street, New York, New York 10032

Received April 19, 2006; Revised Manuscript Received July 7, 2006

ABSTRACT: Solution NMR spin relaxation experiments and classical MD simulations are used to study the dynamics of triosephosphate isomerase (TIM) in complex with glycerol 3-phosphate (G3P). Three regions in TIM exhibit conformational transitions on the μs−ms time scale as detected by chemical exchange broadening effects in NMR spectroscopy: residue Lys 84 on helix C, located at the dimeric interface; active site loop 6; and helix G. The results indicate that the conformational exchange process affecting the residues of loop 6 is the correlated opening and closing of the loop. Distinct processes are responsible for the chemical exchange linebroadening observed in the other regions of TIM. MD simulations confirm that motions of individual residues within the active site loop are correlated and suggest that the chemical exchange processes observed for residues in helix G arise from transitions between 3_{10}- and α-helical structures. The results of the joint NMR and MD study provide global insight into the role of conformational dynamic processes in the function of TIM.

Triosephosphate isomerase (TIM[1]) is the enzyme that catalyzes the reversible isomerization of dihydroxy-acetone phosphate (DHAP) to D-glyceraldehyde 3-phosphate (GAP) during glycolysis. TIM achieves extreme catalytic efficiency for the desired isomerization, with $k_{cat} = 8 \times 10^2\ s^{-1}$ ($k_{cat} = 9 \times 10^3\ s^{-1}$ for the reverse reaction), while suppressing a side reaction leading to the toxic product methyl glyoxal (*1*).

TIM has been the focus of numerous kinetic and structural studies to understand its catalytic efficiency. TIM is a dimer of identical subunits, in which each subunit has an $(\alpha/\beta)_8$ fold, known today as the TIM-barrel fold (*2*−*6*). The monomer structure of TIM is shown in Figure 1. The crystal structures of apo and ligand-bound TIM show small differences apart from the active site loop 6 comprising residues 167−177. The importance of this loop in the catalytic activity of TIM has been highlighted (*7*−*10*). Crystallographic studies have shown that this loop can assume two different configurations: open, leaving the active site accessible to the solvent and substrate, and closed, blocking the entrance to the active site and preventing the loss of the reaction intermediate (*2*, *3*, *5*). The loop has been hypothesized to move as a rigid body because structural changes between open and closed conformations are localized to the hinge residues (*4*, *11*). Deletion of four residues of the loop reduces the catalytic activity of the enzyme by about 5 orders of magnitude and

† This work was supported by National Institutes of Health grant GM59273 (A.G.P). A.G.P. is a member of the New York Structural Biology Center supported by NIH Grant GM66354.

* Corresponding author. Tel: (212) 305-8675. Fax: (212) 305-6949. E-mail: agp6@columbia.edu.

‡ Current address: Biology Department, Center for Biotechnology and Interdisciplinary Studies, Rensselaer Polytechnic Institute, 110 Eighth Street, Troy, NY 12180-3590.

[1] Abbreviations: DHAP, dihydroxy-acetone phosphate; GAP, D-glyceraldehyde 3-phosphate; G3P, glycerol 3-phosphate; MD, molecular dynamics; NMR, nuclear magnetic resonance; QM/MM, quantum mechanical/molecular mechanical; SBMD, stochastic boundary molecular dynamics; TIM, triosephosphate isomerase; TROSY, transverse relaxation optimized spectroscopy.

10.1021/bi060764c CCC: $33.50
Published on Web 08/18/2006

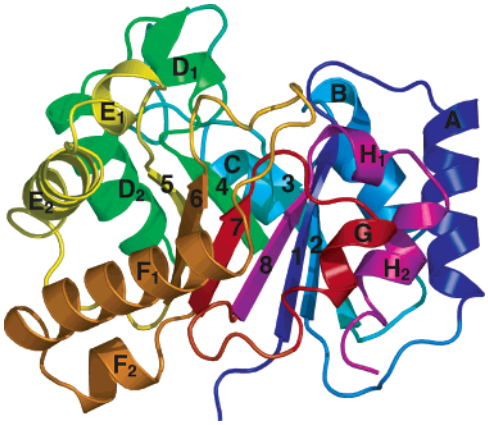

FIGURE 1: TIM monomer structure in the closed state drawn from the protein data bank file 7TIM. The β strands are numbered 1−8, and the α helices are labeled A−H. The eight α/β units are differentially colored. The structural representation was drawn using PyMOL (*37*).

increases the production of the toxic side product by about a factor of 5 because of the loss of the enediol(ate) intermediate (*7*). The rate-limiting step in the isomerization of DHAP to GAP has been shown to be the loss of the product or a slow conformational transition associated with diffusion of the product (*12*). Solid-state NMR (*13*, *14*), solution NMR (*15*), and T-jump relaxation (*16*) spectroscopic studies have shown that loop opening occurs at a rate of $\approx 10^4$ s^{-1} and is rate-limiting or partially rate-limiting. Several classical simulations and combined quantum mechanical/molecular mechanical (QM/MM) studies have had some success elucidating both the details of the catalytic mechanism and the dynamics of TIM (*11*, *17*−*22*).

The conformational flexibility of proteins on microsecond-to-millisecond (μs−ms) time scales directly affects nuclear spin relaxation in NMR spectroscopy. A number of techniques have been developed to quantitatively characterize these motions with a high degree of temporal and atomic resolution (*23*). In the present work, a TROSY Hahn spin−echo solution NMR technique (*24*) is used to globally investigate the conformational dynamics of the (W90Y, W157F) double mutant of yeast TIM on μs−ms time scales. The NMR results provide unequivocal evidence that the residues in active site loop 6 move synchronously, with the same rate constant, between conformations consistent with the open and closed states observed crystallographically. In addition, Lys 84, located on helix C, and residues in helix G also are observed to exhibit conformational transitions distinct from loop opening/closing kinetics. Classical molecular dynamics (MD) simulations are used to assist in the interpretation of NMR results. The MD simulation results suggest that the motion of the active site loop residues is highly correlated, in agreement with the experimental results. The dynamics of helix G suggest a degree of structural plasticity in which its structure fluctuates between 3_{10}- and α-helices.

MATERIALS AND METHODS

NMR Spectroscopy and Data Processing. The sample of W90Y, W157F mutant of yeast TIM was prepared as previously described (*25*). Experimental data were recorded using a sample of [85%-D, U-^{15}N] TIM complexed with glycerol 3-phosphate (G3P) in a 90% H_2O/10% D_2O buffer solution (1 mM TIM, 6 mM G3P, 10 mM CD_3CO_2Na, 0.02 NaN_3 at pH 5.7). At these concentrations of protein and ligand, 96% of TIM is bound to G3P, as calculated for a K_d value of 0.21 ± 0.01 mM measured by NMR titration. Backbone ^{1}H and ^{15}N resonance assignments of G3P-bound TIM were obtained from the assignments of the free protein (BRMB code 7216) by following the chemical shift changes upon titration of the ligand.

All experiments were performed at 800 MHz on a Bruker DRX800 spectrometer equipped with a triple-resonance cryoprobe (New York Structural Biology Center). Data processing was performed using NMRPipe (*26*) and Sparky (*27*) software, along with in-house written programs. The ^{15}N-chemical exchange rate constant, R_{ex}, was determined at 283, 288, 293, and 298 K using a TROSY Hahn spin−echo pulse sequence as described previously (*24*) with a relaxation delay of 10.8 ms. In this experiment, $R_{ex} = R_{2eff} - (\kappa - 1)\eta_{xy}$, in which R_{2eff} is the effective transverse relaxation rate constant, η_{xy} is the transverse dipole−dipole/chemical shift anisotropy relaxation interference rate constant, and κ is an empirical scaling factor determined at each temperature from sites not subject to chemical exchange. Errors in the measurements were estimated from repeated experiments (four sets at 283, 293, and 298 K; three sets at 288 K).

Computer Simulations. The dynamical properties of active site loop 6 and helix G in TIM are the main focus of simulations intended to aid in interpreting the experimental NMR results. Simulations of TIM were performed using two initial sets of coordinates, one for the open state (protein data bank code 1YPI) and one for the closed state of the enzyme bound to the transition state analogue phosphoglycolohydroxamic acid (pdb code 7TIM). In the simulation of the closed state, the inhibitor was removed from the binding pocket. Stochastic boundary molecular dynamics (SBMD) simulations were employed to reduce computational times. The SBMD method has been used in a number of simulation studies of enzyme active sites and has been shown to provide accurate results (*28*, *29*). Briefly, SBMD partitions the system into a reaction zone and a reservoir region. The reaction zone is further separated into a reaction region and buffer region (*28*). The reference point for partitioning the system in the SBMD of TIM was chosen as the C_α of Ala 176 at the *C*-terminus of loop 6; the reaction region, buffer region, and the reservoir region were centered on this reference point. The reaction region was a sphere of radius $r = 14$ Å, the buffer region was defined as the region with $14 < r < 16$ Å, and the reservoir region was defined for $r > 16$ Å. All of the atoms in the reservoir region were deleted. The final simulated system, shown in Figure 2, consisted of 84 protein residues and 304 water molecules, with a total of 2145 atoms. The atoms inside the reaction region were propagated by MD. In the buffer region, particles were propagated by Langevin dynamics with anharmonic restoring forces on heavy atoms derived from the temperature factors of the crystal structure (*28*, *29*). A deformable boundary potential was used to confine water molecules in the reaction zone (*30*). A time step of 1 fs was used in the MD simulation. The friction constant employed in the Langevin dynamics was 250 ps^{-1} for protein atoms and 62 ps^{-1} for water molecules (*29*). After performing minimization and equili-

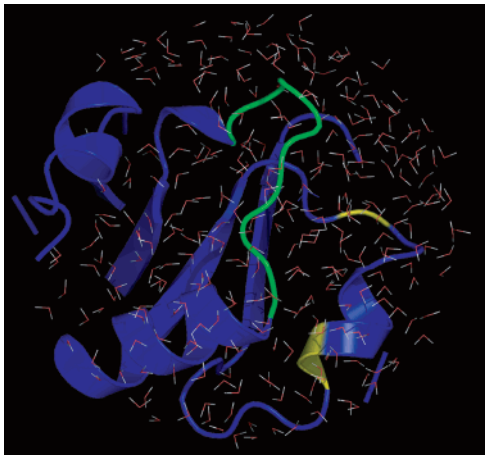

FIGURE 2: Schematic representation of the system included in the stochastic boundary molecular dynamics simulation. The protein is represented as a ribbon, and the water molecules are respresented as stick models. Active site loop 6 is shown in green, and the other residues with R_{ex} values greater than zero are indicated in yellow. The structural representation was drawn using VMD (*38*).

bration for 100 ps at the desired temperature, a production run of 10 ns was collected. Simulations were performed at 300 and 320 K for the open and closed states of the enzyme.

RESULTS AND DISCUSSION

Chemical Shift Perturbation in TIM upon G3P Binding. Figure 3 shows the backbone ^{1}H- and ^{15}N-chemical shift changes observed upon G3P binding. The residues of the protein that show major chemical shift differences are located near or at the region known to interact with G3P, including Asn 10, His 95, Ser 100, Glu 129−Glu 133, Val 167−Ala 186, Asn 213, and Leu 230−Leu 236. Asn 10 and His 95 are known to interact with the sugar moeity of the substrate. Ser 100 and Glu 129−Glu 133 are located on helix D_1 (from residue 95 to 102) and E_1 (from residue 130−137), respectively. Both helices are at the carboxy-terminal end of the barrel forming the active site. The Val 167−Ala 186 region is partly located on the active site loop and on helix F_1. The residues on helix F_1 do not interact directly with the substrate. Their chemical shift changes upon ligand binding are probably related to the motion of loop 6. Asn 213 is at the *C*-terminus of loop 7, and Leu 230−Leu 236 are located on loop 8 and helix H_1. These regions of the protein are known to interact with the phosphate group of the substrate (*3*, *4*). Resonances for Glu 165 (catalytic residue), Gly 210, Ser 211, and Ala 212 (located on loop 7 interacting with the phosphate group) are missing from the NMR spectra, presumably due to the extensive linebroadening arising from chemical exchange (vide infra).

Chemical Exchange in G3P-Bound TIM. Figure 4 shows the chemical exchange contribution to transverse relaxation, R_{ex}, for G3P-bound TIM at 298, 293, 288, and 283 K at B_0 = 18.8 T. At 298 K, Figure 4a, residues Val 167, Trp 168, Leu 174, Thr 177, Asn 213, Phe 220, and Lys 221 have values of R_{ex} that are significantly greater than zero, indicative of chemical exchange processes on μs−ms time scales. Variations in R_{ex} around zero for most other residues reflect site-to-site variations in ^{15}N-chemical shift anisotropy. As the temperature is decreased to 293 K, as shown in Figure 4b, a significant exchange contribution to transverse relaxation is observed for four more residues: Lys 84, Ala 169, Ala 175, and Ile 184. As the temperature is further decreased to 288 K (Figure 4c) and 283 K (Figure 4d), residues Trp 168 and Phe 220 become too broadened for observation. The locations of the exchanging residues in the structure of TIM are shown in Figure 5. Lys 84 is located in helix C, which is at the dimer interface. Val 167, Trp 168, Ala 169, Leu 174, Ala 175, and Thr 177 are located in loop 6. Ile 184 is located in helix F_1, which follows loop 6. Asn 213, Phe 220, and Lys 221 are located at the *N*- and *C*-termini of helix G.

To explore the nature of the chemical exchange process affecting G3P-bound TIM, R_{ex} is plotted in Figure 6 as a function of the chemical shift perturbation observed upon binding of the G3P. Assuming a two-site fast exchange model

$$\lim_{\tau_{cp}\to\infty} R_{ex}(\tau_{cp}) = \frac{p_1 p_2 \Delta\omega^2}{k_{ex}} \qquad (1)$$

in which p_1 and p_2 are the fractional populations of sites 1 and 2 at equilibrium, $\Delta\omega$ is the chemical shift difference between the two sites, and k_{ex} is the exchange rate constant (given by the sum of the forward and reverse kinetic rate constants). A linear correlation is expected for a plot of R_{ex} versus $\Delta\omega^2$ for a set of nuclear spins affected by the same conformational exchange process, characterized by the same fractional populations and rate constant. Figure 6 suggests that the opening/closing of the loop is the conformational

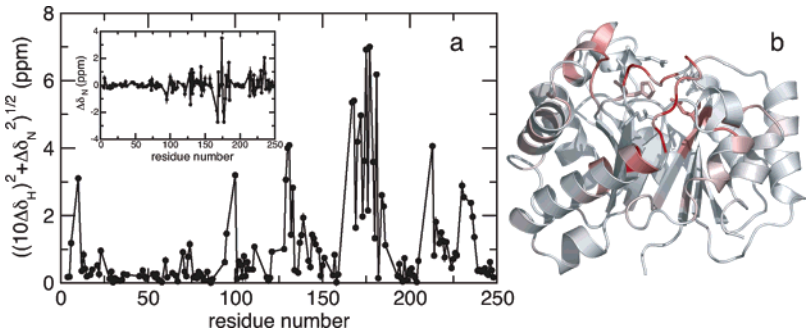

FIGURE 3: Chemical shift changes in TIM upon the binding of G3P. $\Delta\delta_N$ and $\Delta\delta_H$ are the chemical shift changes for ^{15}N and ^1H resonances in ppm, respectively (a). The inset shows the chemical shift changes observed for ^{15}N resonances. The values of $((10\Delta\delta_H^2) + \Delta\delta_N^2)^{1/2}$ are mapped onto the structure of the TIM monomer (b). The color scale goes from white (0 ppm) to red (7.1 ppm). The structural representation was drawn using PyMOL (*37*).

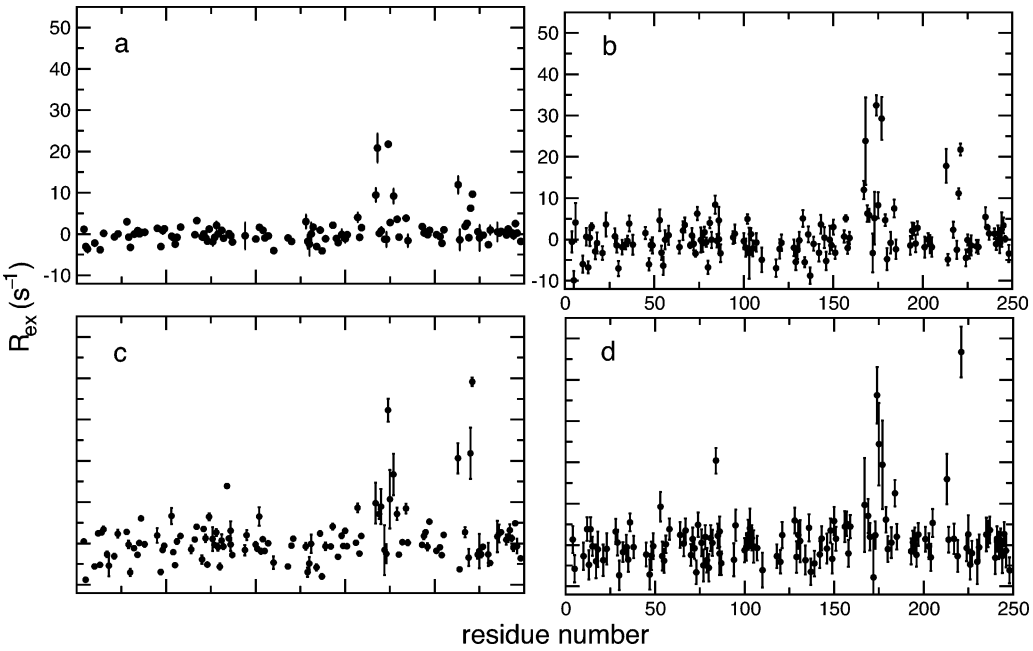

FIGURE 4: Conformational exchange contribution to transverse relaxation, R_{ex}, for G3P-bound TIM at 298 K (a), 293 K (b), 288 K (c), and 283 K (d) at $B_0 = 18.8$ T.

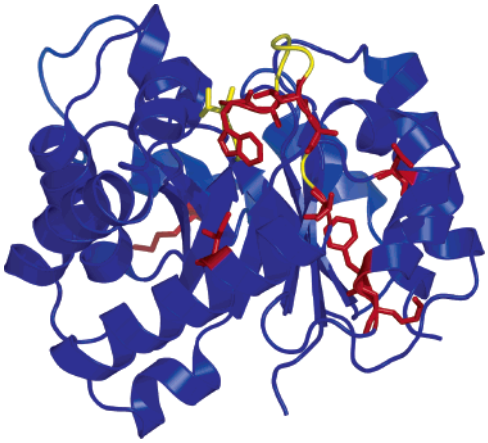

FIGURE 5: Cartoon representation of the apo structure of TIM, highlighting the location of the exchanging residues. Residues with R_{ex} greater than zero are indicated in red. Nonexchanging residues located on loop 6 are colored yellow. The structural representation was drawn using PyMOL(*37*).

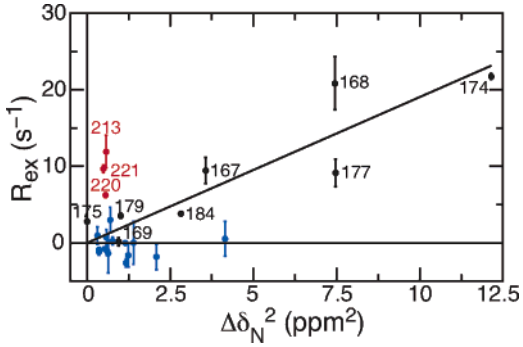

FIGURE 6: Conformational exchange contribution to transverse relaxation, R_{ex}, as a function of the chemical shift changes observed for ^{15}N resonances upon G3P binding at 298 K. A linear correlation is observed for loop 6 residues colored in black (correlation coefficient = 0.9). A linear correlation is not observed for residues 213, 220, and 221, represented in red, indicating that different processes are responsible for chemical exchange linebroadening at these sites. Residues that are not part of loop 6 that show ^{15}N chemical shift changes upon binding G3P are shown in blue. These residues do not exhibit values of R_{ex} that are significantly greater than zero. Residue Lys 84 does not show exchange broadening at 298 K and is not shown.

transition that promotes the chemical exchange contribution to linebroadening for the residues in the loop and residue Ile 184, located in α-helix F_1 immediately following the loop, whereas different conformational transitions affect Lys 84, Asn 213, Phe 220, and Lys 221. Notably, residues whose ^{15}N-chemical shifts are perturbed by binding G3P but are not part of the active site loop (or residue 184) do not exhibit significant chemical exchange broadening. This observation suggests, in agreement with solid-state NMR (*13*, *14*) and optical spectroscopy (*16*), that the observed kinetic process arises from opening and closing transitions of the loop while the enzyme remains saturated with G3P ligand. Furthermore, the observed linear correlation indicates that residues in the loop move synchronously, with the same rate constant, k_{ex}. This result confirms the original hypothesis that the loop moves as a rigid body (*4*, *11*). Assuming site populations of 0.04 and 0.96 for the open and closed states, respectively, at the used concentration of G3P, a value of k_{ex} equal to 3500 ± 200 s^{-1} is calculated for loop motion from the fit of the loop data at 288 K. This value of k_{ex} is in agreement with that previously obtained for Trp 168 using solid state ^2H NMR and ^{19}F solution state NMR (*14*, *15*).

Temperature Dependence of R_{ex}. The temperature dependence of R_{ex} provides information on the apparent activation barrier, E_a, associated with the conformational transitions that determine R_{ex} (*31*−*33*). Assuming a two-state fast exchange model with $p_1 > p_2$, the apparent activation energy is given by

$$\frac{d(\ln R_{ex})}{d(1/RT)} = E_a = \Delta H^{\ddagger} + \Delta H_{12}(1 - 3p_1) \qquad (2)$$

in which R is the universal gas constant, T is the temperature,

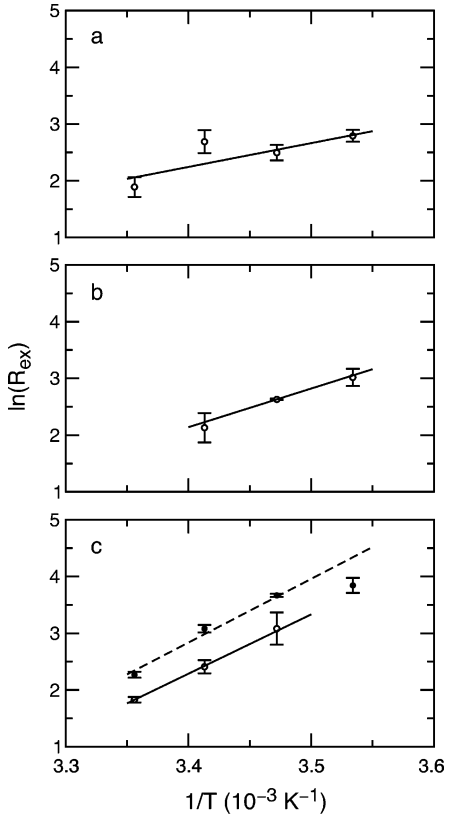

FIGURE 7: Temperature dependence of conformational exchange contribution to transverse relaxation, R_{ex}. Arrhenius plots are shown for the average value of R_{ex} in loop 6 (a), for Lys 84 (b), Phe 220 (solid line and ○) and Lys 221 (dashed line and ●) (c).

Table 1: Apparent Activation Energies for Chemical Exchange in TIM

residue	E_a (kJ/mol)
Lys 84	57 ± 11
loop 6[a]	30 ± 10
Asn 213	27 ± 25
Phe 220	87 ± 6
Lys 221	93 ± 21

[a] The apparent activation energy of loop 6 has been evaluated from the fit of $\ln(R_{ex})$ versus $1/T$, using the average value of R_{ex} calculated for the exchanging residues in loop 6 (Val 167, Trp 168, Ala 169, Leu 174, Ala 175, and Thr 177) and Ile 184.

$\Delta H^{\ddagger}$ is the activation enthalpy for the forward reaction, and ΔH_{12} is the enthalpic difference between exchanging states 1 and 2 (*31*, *32*). As shown in Figure 4, chemical exchange linebroadening increases with decreasing temperature, indicating that the exchange process is intermediate to fast on the chemical shift time scale. Figure 7 depicts the Arrhenius plots for residues in G3P-bound TIM and shows a linear dependence of $\ln R_{ex}$ upon $1/T$, over the temperature range studied. The apparent activation energies, E_a, derived from the slope of the Arrhenius plots are presented in Table 1. The apparent activation energy for the opening of loop 6 has been evaluated using the average R_{ex} value of the exchanging residues in the loop and Ile 184 because the same activation process determines chemical exchange in these residues, as previously discussed. Eq 2 shows that the apparent activation energy measured from the temperature dependence of R_{ex} always yields an underestimation of the enthalpy of activation for the reaction. For example, assuming a major state population of 96% and no entropic difference between the two exchanging states, E_a underestimates $\Delta H^{\ddagger}$ by about 15 kJ/mol, yielding an estimate of $\Delta H^{\ddagger} = 45$ kJ/mol. Thus, the E_a value estimated for the active site loop motion is in reasonable agreement with the value of $\Delta H^{\ddagger}_{open}$ of 59 ± 10 kJ/mol derived from temperature-jump relaxation spectroscopic studies of G3P bound TIM (*16*). The values of the apparent activation barriers, E_a, obtained for Phe 220 and Lys 221 suggest that a second process distinct from loop 6 dynamics determines chemical exchange linebroadening in these adjacent residues, while a third conformational process affects residue Lys 84. The large uncertainty in the value of E_a derived for Asn 213 makes any interpretation inconclusive.

Dynamics of the Active Site Loop. The crystal structures of apo and bound TIM show that several hydrogen bonds stabilize loop 6 in the open and/or closed conformations. Intraloop hydrogen bonds, from the backbone amide nitrogens of Ala 169 and Ile 170 to the carbonyl groups of Pro 166 and Val 167, respectively, and from the hydroxyl group of Thr 172 to the amide nitrogen of Leu 174 and to the carbonyl of Trp 168, appear to stabilize the loop structure. In the open configuration, the indole nitrogen of Trp 168 is hydrogen bonded to the hydroxyl group of Tyr 164. This hydrogen bond is broken, and a new one is formed with the carboxyl group of Glu 129 when the loop is in the closed configuration. Two additional hydrogen bonds are formed between the hydroxyl groups of Tyr 208 and Ser 211 and the amide nitrogens of Ala 176 and Gly 173, respectively, upon loop closure. The presence of these hydrogen bonds that stabilize the closed/open states and the distance between the loop residues and Tyr 208 were monitored during the simulation.

Simulations that started from the closed conformation of loop 6 at 300 K exhibited loop opening, whereas simulations that started from the open state exhibited transitions of the loop between closed and open conformations without fully closing. Similar behavior was observed in the trajectories run at 320 K. The distance between the C_α atoms of the residues of loop 6 and Tyr 208 was used to monitor the motion of loop 6, as shown in Figure 8. The results of the simulations indicate that the motions of the residues of loop 6 are highly correlated.

In the simulation that started from the closed state, the hydrogen bond between Trp 168 and Glu 129 was present 15% of the time, and the hydrogen bond between Tyr 208 and Ala 176 was present 65% of the time, whereas the hydrogen bond between Ser 211 and Gly 173 was present 3% of the time. This result indicates that the opening of the loop causes the breaking of the hydrogen bonds at different times, with the Tyr 208−Ala 176 hydrogen bond being the last. The intraloop hydrogen bonds that stabilize the overall structure of the loop are intermittently present for the entire length of the simulation run: Ile 170−Val 169 and Ala 169−Pro 166 66% and 24% of the time, respectively. The formation of other intraloop hydrogen bonds is observed along the trajectory for the side chain of Thr 172 with Trp 168 or Ala 169, Leu 174−Thr 172, Leu 174−Trp 168. The formation of a hydrogen bond between the side chain nitrogen of Trp 168 and the hydroxyl group of Tyr 164, characteristic of the open state, is observed 2% of the time, indicating that the indole ring repositions itself upon loop opening.

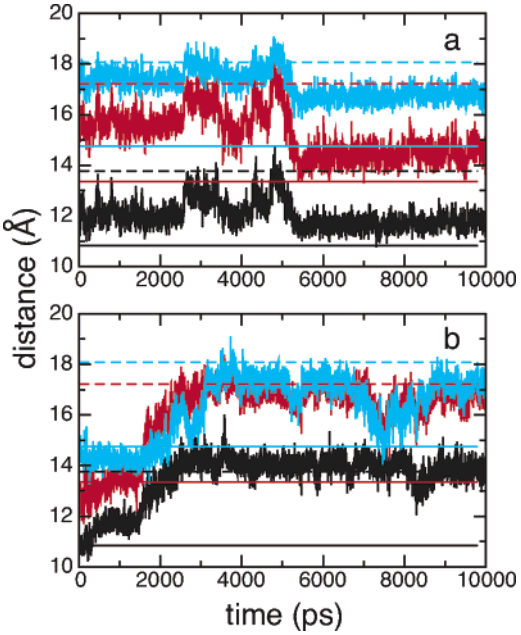

FIGURE 8: Distance between the C_α atoms of the residues of loop 6 and Y208 is represented as a function of time for trajectories starting from the closed (pdb 7TIM) (a) and open (pdb 1YPI) (b) states of TIM. In a and b, the distances between Tyr 208 and Ile 170, Gly 171, and Thr 172 are depicted in black, red, and cyan, respectively. Solid and dashed lines show the value of the distances in the crystal structures of the closed (—) and open (---) states.

In the simulation that started from the open state, the indole ring of Trp 168 samples both open and closed conformations, forming a hydrogen bond with the side chain nitrogen to Tyr 164 and Glu 129, 66% and 15% of the time, respectively. The hydrogen bonds between Tyr 208 and Ala 176 and between Ser 211 and Gly 173, signatures of the closed states, are seldom observed (the frequency is less than 1%). Intraloop hydrogen bonds are present throughout the entire trajectory (although not continuously): Ala 169−Pro 166, Ile 170−Pro 166, Thr 172−Trp 168, Gly 173−Trp 168, Leu 174−Trp 168, Leu 174−Thr 172 have frequencies of 47%, 76%, 0.5%, 0.3%, 0.3%, and 0.2%, respectively.

An analysis of the backbone dihedral angles, ϕ and ψ, and of the Cα pseudo dihedral angles reveals a certain degree of flexibility of the loop backbone upon opening under the studied conditions. The pseudodihedral angles, Θ, are defined by the Cα of residues $i-1$, i, $i+1$, and $i+2$, and represent the rotation around the central residues i and $i+1$ (*11*). The differences of the Cα pseudodihedral angles between the X-ray structures of free and bound TIM are highest for residues at the hinges of the loop (166,174, 175, and 175) and are close to zero for all the other residues in the loop (*11*). The MD simulations indicate that the most flexible region of the loop is centered around Gly 173 and consists of residues 170−175, near the *C*-terminus of the loop. This result is in agreement with previous computer simulation studies that identified the motion of Gly 173 among the initial steps in the opening of the active site loop (*22*). Figure 9a shows the root-mean-square fluctuations of the pseudodihedral angle of residues 163−179 of TIM for the simulation that started from the closed and open configurations of the enzyme, respectively. Figure 9 parts b and c show the values of the pseudodihedral angles for residues 171−175 at time t minus their values in the X-ray structures used as the initial

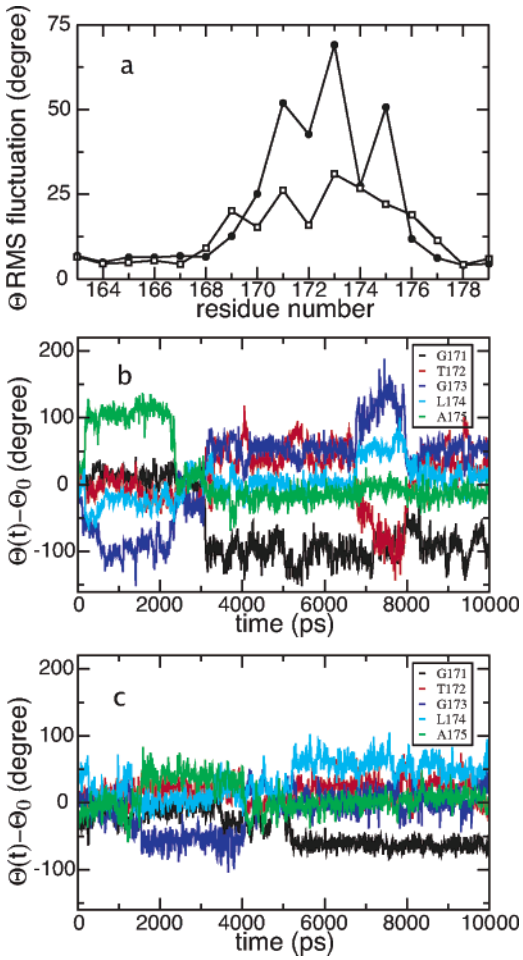

FIGURE 9: Cα pseudodihedral angle, Θ, defined by the Cα of residues $i-1$, i, $i+1$, $i+2$. (a) RMS fluctuations of Θ as a function of the residue number for the trajectories that started from the closed and open states at 300 K represented as closed and open symbols, respectively. The difference $\Theta(t)-\Theta_0$ as a function of time for the trajectory that started from the closed state (b) and from the open state (c). Θ_0 is the value of the pseudodihedral angle Θ in the X-ray structure used as the starting configuration of the trajectory.

configuration of the trajectory. These residues, which display the highest values of RMS fluctuations, are undergoing several correlated main chain dihedral angle transitions along the trajectory that started from the closed state. Fewer transitions, also correlated, are observed in the trajectory that started from the open state.

Dynamics of Loop 7 and Helix G. The flexibility of loop 7 has been noted by Wierenga and co-workers in crystallographic studies of trypanosomal TIM (*34*). These studies indicate that upon ligand binding, the position of loop 7 shifts by about 1.5 Å. This change allows the formation of a hydrogen bond between the backbone amide nitrogen of Ser 213 (corresponding to Ser 211 in yeast TIM) and the phosphate group of the ligand. In addition, in the closed configuration, the side chain OG of Ser 213 forms hydrogen bonds with residues in the active site loop, Gly 173 and Gly 175 (corresponding to Gly 171 and Gly 173 in yeast TIM). In yeast TIM, the configurational change of loop 7 promoted by ligand binding is similar to that observed in trypanosomal TIM. The change in the positions of the Cα atoms of loop 7 amounts to about 1 Å, and the closed conformations of yeast TIM and trypanosomal TIM are nearly identical (*35*).

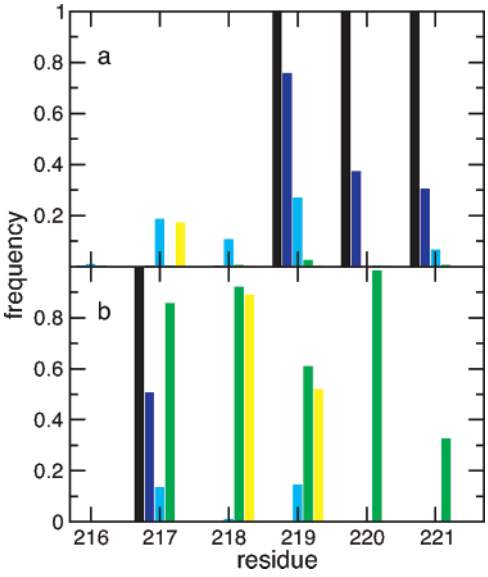

FIGURE 10: Frequency of formation of hydrogen bonds in helix G. (a) Frequency of the *i*, *i* + 3 hydrogen bonds is represented for the X-ray structure (black), for the MD trajectory that started from the closed configuration at 300 K (blue) and at 320 K (green), and for the MD trajectory that started from the open configuration at 300 K (cyan) and at 320 K (yellow). (b) Frequency of the *i*, *i* + 4 hydrogen bonds is represented for the X-ray structure (black), the MD trajectory that started from the closed configuration at 300 K (blue) and at 320 K (green), and for the MD trajectory that started from the open configuration at 300 K (cyan) and at 320 K (yellow). The residue number indicates the amide group involved in the hydrogen bond.

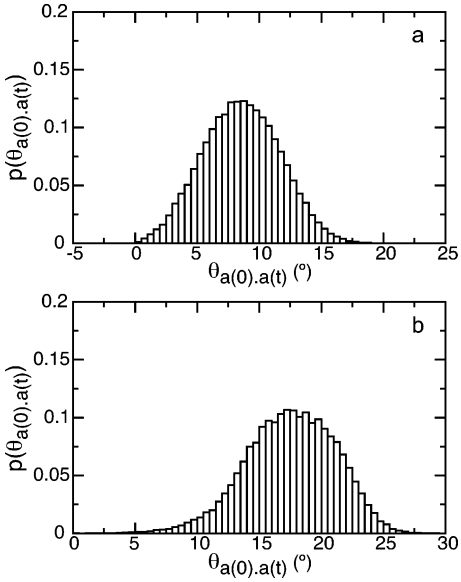

FIGURE 11: Distribution of the angle between the axis of helix G in the crystal structure ($t = 0$) and at time t along the simulation trajectory starting from the closed state (pdb 7TIM) (a) and along the trajectory starting from the open state (pdb 1YPI) (b).

The hydrogen-bond patterns found in the crystal structure of both the apo and bound state classify helix G as a 3_{10}-helix, as shown by the black bars in Figure 10. The presence of an *i*, *i* + 4 hydrogen bond at the *N*-terminus of the helix, between the amide group of Ala 217 and the carbonyl group of Asn 213, is a relatively common occurrence in 3_{10}-helices (*36*). A different hydrogen-bond pattern is observed in the MD simulations, as shown in Figure 10. The trajectory that started from the closed state configuration at 300 K, represented in blue in Figure 10, shows a hydrogen-bond pattern that is most similar to the one found in the X-ray structures. The *C*-terminus of the helix, Lys 221, shows a propensity to be hydrogen bonded to Thr 219 with a frequency of 5%. As the temperature is increased to 320 K, the hydrogen-bond pattern is typical of a α-helix, as shown in green in Figure 10. The MD trajectories that started from the open state configuration present both i,i+3 and i,i+4 hydrogen-bond patterns, as shown in Figure 10, with a higher propensity for i, i+4 at 320 K, (yellow bars). At 300 K, the *C*-terminus of the helix, Lys 221, is hydrogen bonded to Thr 219 with a frequency of 30%. The average values of the backbone dihedral angles, ϕ and ψ, are intermediate between the ideal α- and 3_{10}-helical values (not shown). In addition, the orientation of the helix changed as a function of time as indicated by the distribution of angles of the helix axis shown in Figure 11. The computer simulation study of TIM indicates that the structure of helix G is dynamical, transitioning between a 3_{10}-helix and an α-helix, with a coupled motion of the helix axis. Residues Asn 213, Phe 220, and Lys 221, located at the *N*- and *C*-termini of this helix, are characterized by chemical exchange processes that are distinct from the motions of loop 6. The nominal time scale of the motional processes investigated in the MD simulation is shorter than the time scale of the configurational transitions characterizing chemical exchange linebroadening; nonetheless, the simulation suggests a degree of structural plasticity in helix G that may provide the mechanism for the experimentally observed chemical exchange phenomena. Further studies are required to more definitively determine the nature of these motional processes.

CONCLUSIONS

Solution NMR spin relaxation experiments and classical MD simulations have been used to study the dynamics of TIM. Three regions in TIM have been identified experimentally as undergoing conformational transitions on the μs−ms time scale: residue Lys 84 on helix C, located at the dimeric interface; the active site loop 6; and helix G. The results indicate that the conformational exchange process affecting the residues of loop 6 is the opening/closing of the loop. Most significantly, the exchanging residues in loop 6 have the same site populations and rate constant for the opening/closing transition, providing unequivocal evidence that the motions of the loop residues are correlated. In contrast, hitherto unsuspected processes are responsible for the chemical exchange linebroadening observed in the other regions of TIM. The results of the MD simulations confirm that active site loop motion is correlated and suggest that the chemical exchange processes observed for residues in helix G may arise from transitions between 3_{10}- and α-helical structures. In particular, the hydrogen bonds important in the stabilization of the closed conformation break at different times. Gly 173−Ser 211 is the first, and Tyr 208−Ala 176 is last to be broken. The loop is most flexible around residue Gly 173.

ACKNOWLEDGMENT

We thank Jianpeng Ma and Ann McDermott for helpful discussions.

SUPPORTING INFORMATION AVAILABLE

Chemical shift assignments for G3P-bound TIM and conformational exchange contribution to transverse relaxation, R_{ex}, for G3P-bound TIM at 298, 293, 288, and 283 K at $B_0 = 18.8$ T. This material is available free of charge via the Internet at http://pubs.acs.org.

REFERENCES

1. Richard, J. P. (1984) Acid−base catalysis of the elimination and isomerization-reactions of triose phospate, *J. Am. Chem. Soc. 106*, 4926−4936.
2. Lolis, E., Alber, T., Davenport, R. C., Rose, D., Hartman, F. C., and Petsko, C. A. (1990) Structure of yeast triosephosphate isomerase at 1.9 Å resolution, *Biochemistry 29*, 6609−6618.
3. Lolis, E., and Petsko, C. A. (1990) Crystallographic analysis of the complex between triosephosphate isomerase and 2-phosphoglycolate at 2.5 Å resolution: implications for catalysis, *Biochemistry 29*, 6619−6625.
4. Davenport, R. C., Bash, P. A., Seaton, B. A., Karplus, M., Petsko, C. A., and Ringe, D. (1991) Structure of the triosephosphate isomerase-phosphoglycolohydroxamate complex: an analogue of the intermediate on the reaction pathway, *Biochemistry 30*, 5821−5826.
5. Wierenga, R. K., Borcher, T. V., and Noble, M. E. M. (1992) Crystallographic binding studies of triosephosphate isomerase: conformational changes induced by substrate and substrate-analogues, *FEBS lett. 307*, 34−39.
6. Jogl, G., Rozovsky, S., McDermott, A. E., and Tong, L. (2003) Optimal alignment for enzymatic proton transfer: structure of the Michaelis complex of triosephosphate isomerase at 1.2 Å resolution, *Proc. Natl. Acad. Sci. U.S.A. 100*, 50−55.
7. Pompliano, D. L., Peyman, A., and Knowles, J. R. (1990) Stabilization of a reaction intermediate as a catalytic device: definition of the functional-role of the flexible loop in triosephosphate isomerase, *Biochemistry 29*, 3186−3194.
8. Sampson, N. S., and Knowles, J. R. (1992) Segmental movement: definition of the structural requirements for loop closure in catalysis by triosephosphate isomerase, *Biochemistry 31*, 8482−8487.
9. Xiang, J., Sun, J., and Sampson, N. S. (2001) The importance of hinge sequence for loop function and catalytic activity in the reaction catalyzed by triosephosphate isomerase, *J. Mol. Biol. 307*, 1103−1112.
10. Xiang, J., Jung, J., and Sampson, N. S. (2004) Entropy effects on protein hinges: the reaction catalyzed by triosephosphate isomerase, *Biochemistry 43*, 11436−11445.
11. Joseph, D., Petsko, G. A., and Karplus, M. (1990) Anatomy of a conformational change: Hinged "lid" motion of the triosephosphate isomerase loop, *Science 249*, 1425−1428.
12. Albery, W. J., and Knowles, J. R. (1976) Free-energy profile of the reaction catalyzed by triosephosphate isomerase, *Biochemistry 15*, 5627−5631.
13. Williams, J. C., and McDermott, A. E. (1995) Dynamics of the flexible loop of triosephosphate isomerase: The loop motion is not ligand gated, *Biochemistry 34*, 8309−8319.
14. Rozovsky, S., and McDermott, A. E. (2001) The time scale of the catalytic loop motion in triosephosphate isomerase, *J. Mol. Biol. 310*, 259−270.
15. Rozovsky, S., Jogl, G., Tong, L., and McDermott, A. E. (2001) Solution-state NMR investigations of triosephosphate isomerase active site loop motion: ligand release in relation to active site loop dynamics, *J. Mol. Biol. 310*, 271−280.
16. Desamero, R., Rozovsky, S., Zhadin, N., McDermott, A., and Callender, R. (2003) Active site loop motion in triosephosphate isomerase: T-jump relaxation spectroscopy of thermal activation, *Biochemistry 42*, 2941−2951.
17. Cui, Q., and Karplus, M. (2003) Catalysis and specificity in enzymes: a study of triosephosphate isomerase and comparison with methyl glyoxal synthase, *Adv. Protein Chem. 66*, 315−372.
18. Guallar, V., Jacobson, M., McDermott, A., and Friesner, R. A. (2004) Computational modeling of the catalytic reaction in triosephosphate isomerase, *J. Mol. Biol. 337*, 227−239.
19. Brown, F. K., and Kollman, P. A. (1987) Molecular dynamics simulations of "loop closing" in the enzyme triose phosphate isomerase, *J. Mol. Biol. 198*, 533−546.
20. Karplus, M., Evanseck, J. D., Joseph, D., Bash, P. A., and Field, M. J. (1992) Simulation analysis of triose phosphate isomerase: conformational transition and catalysis, *Faraday Discuss. 93*, 239−248.
21. Wade, R. C., Luty, B. A., Demchuk, E., Madura, J. D., Davis, M. E., Briggs, J. M., and McCammon, J. A. (1994) Simulation of enzyme−substrate encounter with gated active sites, *Nat. Struct. Biol. 1*, 65−69.
22. Derreumaux, P., and Schlick, T. (1998) The loop opening/closing motion of the enzyme triosephosphate isomerase, *Biophys. J. 74*, 72−81.
23. Palmer, A. G. (2004) NMR characterization of the dynamics of biomacromolecules. *Chem. Rev. 104*, 3623−3640.
24. Wang, C., Rance, M., and Palmer, A. G. (2003) Mapping chemical exchange in proteins with MW > 50 kD, *J. Am. Chem. Soc. 125*, 8968−8969.
25. Rance, M., Loria, J. P., and Palmer, A. G. (1999) Sensitivity improvement of transverse relaxation-optimized spectroscopy, *J. Magn. Reson. 136*, 92−101.
26. Delaglio, F., Grzesiek, S., Vuister, G. W., Zhu, G., Pfeifer, J., and Bax, A. (1995) NMRPipe: a multidimensional spectral processing system based on Unix pipes, *J. Biomol. NMR 6*, 277−293.
27. Goddard, T. D., and Kneller, D. G. *SPARKY 3*, University of California, San Francisco, CA.
28. Brooks, C. L., Brünger, A., and Karplus, M. (1985) Active site dynamics in protein molecules: A stochastic boundary molecular dynamics approach, *Biopolymers 24*, 843−865.
29. Brooks, C. L., and Karplus, M. (1989) Solvent effect on protein motion and protein effects on solvent motion, *J. Mol. Biol. 208*, 159−181.
30. Brooks, C. L., and Karplus, M. (1983) Deformable stochastic boundaries in molecular dynamics, *J. Chem. Phys. 79*, 6312−6325.
31. Mandel, A. M., Akke, M., and Palmer, A. G. (1996) Dynamics of Ribonuclease H: Temperature dependence of motions in multiple time scales, *Biochemistry 35*, 16009−16023.
32. Evenäs, J., Forsén, S., Malmendal, A., and Akke, M. (1999) Backbone dynamics and energetics of a calmodulin domain mutant exchanging between closed and open conformations, *J. Mol. Biol. 289*, 603−617.
33. Butterwick, J. A., Loria, J. P., Astrof, N. S., Kroenke, C. D., Cole, R., Rance, M., and Palmer, A. G. (2004) Multiple time scale backbone dynamics of homologous thermophilic and mesophilic ribonuclease HI enzymes, *J. Mol. Biol. 339*, 855−871.
34. Wierenga, R. K., Noble, M. E. M., Vriend, G., Nauche, S., and Hol, W. G. J. (1991) Refined 1.83 Å crystal structure of trypanosomal triosephosphate isomerase crystallized in the presence of 2.4 M ammonium sulphate, *J. Mol. Biol. 220*, 995−1015.
35. Wierenga, R. K., Noble, M. E. M., and Davenport, R. C. (1992) Comparison of the refined crystal structures of liganded and unliganded chicken, yeast and trypanosomal triosephosphate isomerase, *J. Mol. Biol. 224*, 1115−1126.
36. Doig, A. J., MacArthur, M. W., Stapley, B. J., and Thornton, J. M. (1997) Structures of N-termini of helices in proteins, *Protein Sci. 6*, 147−155.
37. DeLano, W. L. (2002) *The PyMOL Molecular Graphics System* (DeLano Scientific, San Carlos, CA). http://www.pymol.org.
38. Humphrey, W., Dalke, A., and Schulten, K. (1996) VMD−Visual molecular dynamics, *J. Mol. Graphics 14*, 33−38.

BI060764C